



The Dynamics of Two Coupled van der Pol Oscillators with Delay Coupling

STEPHEN WIRKUS

Department of Mathematics and Statistics, California State Polytechnic University–Pomona, Pomona, CA 91768, U.S.A.

RICHARD RAND

Department of Theoretical and Applied Mechanics, Cornell University, Ithaca, NY 14853, U.S.A.

(Received: 2 August 2000; accepted: 11 April 2001)

Abstract. We investigate the dynamics of a system of two van der Pol oscillators with delayed velocity coupling. We use the method of averaging to reduce the problem to the study of a slow-flow in three dimensions. We study the steady state solutions of this slow-flow, with special attention given to the bifurcations accompanying their change in number and stability. We compare these stability results with numerical integration of the original equations and show that the two sets of results are in excellent agreement under certain parameter restrictions. Our interest in this system is due to its relevance to coupled laser oscillators.

Keywords: Differential-delay equations, coupled oscillators, bifurcations, phase-locking.

1. Introduction

This work is concerned with the mutual interaction of two limit cycle oscillators. It is motivated by applications to laser dynamics and, more generally, to microwave oscillators [1–4]. When two microwave oscillators operate physically close to one another, the output signal of each may affect the behavior of the other. Since the frequencies are above the 10 GHz range, the time for light to travel from one oscillator to the other, a distance of the order of centimeters, represents a substantial portion of the period of the uncoupled microwave oscillator. This immediately leads to the inclusion of delay effects in the coupling terms.

In this paper we investigate the dynamics of two weakly coupled van der Pol oscillators in which the coupling terms have time delay τ . The coupling has been chosen to be via the first derivative terms because this form of coupling occurs in radiatively coupled microwave oscillator arrays [1, 3, 4]. We use the method of averaging to obtain an approximate simplified system of three slow-flow equations and then investigate the stability and bifurcation of their equilibria (corresponding to periodic motions in the original system). Experimentalists Lynch and York consider the van der Pol oscillator as a generic microwave oscillator and state that ‘in practice, any useful operational mode of a system of coupled oscillators where coherent power combining is desired must exhibit some type of stable periodicity’ [1]. We then compare these results with the numerical integration of the original differential delay equations.

This work is an extension of previous papers by the present authors [5, 6] and is also related to previous studies of coupled van der Pol oscillators in which the coupling terms omitted delay effects [7–10].

2. Derivation of Slow-Flow Equations

We investigate two van der Pol oscillators with delay coupling [1, 4]:

$$\ddot{x}_1 + x_1 - \varepsilon (1 - x_1^2) \dot{x}_1 = \varepsilon \alpha \dot{x}_2 (t - \tau), \quad (1)$$

$$\ddot{x}_2 + x_2 - \varepsilon (1 - x_2^2) \dot{x}_2 = \varepsilon \alpha \dot{x}_1 (t - \tau), \quad (2)$$

where α is a coupling parameter, τ is the delay time, and where $\varepsilon \ll 1$. When $\varepsilon = 0$, the system reduces to $\ddot{x}_i + x_i = 0$, $i = 1, 2$, with solution:

$$x_i = R_i \cos(t + \theta_i), \quad \dot{x}_i = -R_i \sin(t + \theta_i). \quad (3)$$

For $\varepsilon > 0$, we look for a solution in the form (3) but treat R_i and θ_i as time dependent. Variation of parameters gives the following equations on R_i and θ_i :

$$\dot{R}_i = -\varepsilon \sin(t + \theta_i) F_i, \quad R_i \dot{\theta}_i = -\varepsilon \cos(t + \theta_i) F_i, \quad (4)$$

where $F_i = (1 - x_i^2) \dot{x}_i + \alpha \dot{x}_j (t - \tau)$, $i, j = 1, 2$. For small ε we use the method of averaging, replacing the right-hand sides of (4) by their averages over one period of the $\varepsilon = 0$ system:

$$\dot{R}_i \approx -\varepsilon \frac{1}{2\pi} \int_0^{2\pi} \sin(t + \theta_i) F_i dt, \quad (5)$$

$$R_i \dot{\theta}_i \approx -\varepsilon \frac{1}{2\pi} \int_0^{2\pi} \cos(t + \theta_i) F_i dt, \quad (6)$$

in which

$$F_i = [1 - R_i^2 \cos^2(t + \theta_i)] [-R_i \sin(t + \theta_i)] + \alpha [-\tilde{R}_j \sin(t - \tau + \tilde{\theta}_j)], \quad (7)$$

where $\tilde{R} = R(t - \tau)$ and $\tilde{\theta} = \theta(t - \tau)$. Evaluating the integrals $\oint \cos(t + \theta_i) F_i dt$ and $\oint \sin(t + \theta_i) F_i dt$ gives

$$\dot{R}_i = \frac{\varepsilon}{2} R_i \left(1 - \frac{R_i^2}{4}\right) + \frac{\varepsilon \alpha}{2} \tilde{R}_j \cos(\theta_i - \tilde{\theta}_j + \tau), \quad (8)$$

$$R_i \dot{\theta}_i = -\frac{\varepsilon \alpha}{2} \tilde{R}_j \sin(\theta_i - \tilde{\theta}_j + \tau). \quad (9)$$

Equations (8–9) show that $\dot{R}_i, \dot{\theta}_i$ are $O(\varepsilon)$. We now Taylor expand \tilde{R}_i and $\tilde{\theta}_i$:

$$\tilde{R}_i = R_i(t - \tau) = R_i(t) - \tau \dot{R}_i(t) + \tau^2 \ddot{R}_i(t) + \dots, \quad (10)$$

$$\tilde{\theta}_i = \theta_i(t - \tau) = \theta_i(t) - \tau \dot{\theta}_i(t) + \tau^2 \ddot{\theta}_i(t) + \dots. \quad (11)$$

Equations (10) and (11) indicate that we can replace $\tilde{R}_i, \tilde{\theta}_i$ by R_i, θ_i in Equations (8) and (9) since $\dot{R}_i(t), \dot{\theta}_i(t)$ and $\ddot{R}_i(t), \ddot{\theta}_i(t)$ in (10), (11) are $O(\varepsilon)$ and $O(\varepsilon^2)$ respectively, from Equations (8) and (9). This reduces an infinite dimensional problem in functional analysis to a finite dimensional problem by assuming the product $\varepsilon \tau$ is small. (Note that we do not assume

a small delay τ .) This key step enables us to handle the original system, a differential delay equation, as a system of differential equations [1–4]. Note that if terms of $O(\varepsilon^2)$ were retained in Equations (10) and (11), then the resulting differential equations would be of second order. Thus extending the expansion to higher order in ε has the unusual effect of profoundly changing the nature of the approximate system to be solved. Nevertheless, the $O(\varepsilon)$ truncation studied in this work is valid for small values of $\varepsilon\tau$, as demonstrated by comparison of the subsequent slow-flow analysis with numerical integration of the original differential delay equations (1–2).

We let $T = t/\varepsilon$ be the new time scale. Setting $\phi = \theta_1 - \theta_2$, we then obtain

$$\dot{R}_1 = \frac{1}{2} \left[R_1 \left(1 - \frac{R_1^2}{4} \right) + \alpha R_2 \cos(\phi + \tau) \right], \tag{12}$$

$$\dot{R}_2 = \frac{1}{2} \left[R_2 \left(1 - \frac{R_2^2}{4} \right) + \alpha R_1 \cos(\phi - \tau) \right], \tag{13}$$

$$\dot{\phi} = \frac{\alpha}{2} \left[-\frac{R_2}{R_1} \sin(\phi + \tau) - \frac{R_1}{R_2} \sin(\phi - \tau) \right]. \tag{14}$$

These are the slow-flow equations which we will examine in the remainder of the paper.

Note that R_1 and R_2 are nonnegative and the vector field associated with Equations (12–14) is periodic in ϕ . Thus the phase space is $R^+ \times R^+ \times S^1$. The slow-flow is invariant under the three transformations:

$$(R_1, R_2, \phi) \mapsto (R_2, R_1, -\phi), \tag{15}$$

$$\phi \mapsto \phi + \pi, \quad \alpha \mapsto -\alpha, \tag{16}$$

$$\phi \mapsto \phi + \pi, \quad \tau \mapsto \tau + \pi, \quad \cos \tau \mapsto -\cos \tau. \tag{17}$$

Equations (16) and (17) show that another invariance involving only parameters is

$$\alpha \mapsto -\alpha, \quad \tau \mapsto \tau + \pi, \quad \cos \tau \mapsto -\cos \tau. \tag{18}$$

Equation (18) shows that we may assume $\alpha > 0$ without loss of generality, since the phase flow for a negative value of α is identical to that of the corresponding positive value of α with the sign of $\cos \tau$ reversed.

3. Stability of the In-Phase Mode

Equations (12–14) possess the following equilibrium point which corresponds to the in-phase mode $x_1 \equiv x_2$ in (1–2):

$$R_1 = R_2 = 2 \sqrt{1 + \alpha \cos \tau}, \phi = 0, \quad 1 + \alpha \cos \tau > 0. \tag{19}$$

Notice that Equations (19) indicate that the amplitudes R_i approach zero as $1 + \alpha \cos \tau$ approaches zero, and that these amplitudes remain zero for $1 + \alpha \cos \tau \leq 0$. This result is known as *amplitude death* [11, 12]. Thus the in-phase mode is predicted to come into existence as we cross the curve $\alpha = -1/\cos \tau$ in the $\cos \tau - \alpha$ parameter plane. This bifurcation is accompanied by a change in stability of the trivial solution $x_1 \equiv x_2 \equiv 0$. In order to show this

we must return to the original differential delay equations (1–2), since the slow-flow (12–14) is singular for $R_1 = R_2 = 0$. Linearizing Equations (1–2) about the trivial solution, we may obtain the condition for a change in stability of $x_1 \equiv x_2 \equiv 0$ by assuming a solution of the form $e^{i\omega t}$. Equating real and imaginary parts of the corresponding characteristic equation, we obtain

$$\cos \omega \tau = -\frac{1}{\alpha}, \quad \sin \omega \tau = \frac{1 - \omega^2}{\varepsilon \alpha \omega}. \quad (20)$$

In the small ε limit, the second of Equations (20) gives that $\omega = 1$, and then the first of Equations (20) gives $\alpha = -1/\cos \tau$, in agreement with the birth of the in-phase mode, cf. Equation (19).

In order to determine the stability of the in-phase mode, we examine the eigenvalues λ of the Jacobian matrix of the right-hand side of Equations (12–14) evaluated at the equilibrium (19). These satisfy the equation:

$$\begin{aligned} \lambda^3 + \lambda^2 (2 + 4 \alpha \cos \tau) + \lambda (1 + 5 \alpha \cos \tau + \alpha^2 + 4 \alpha^2 \cos^2 \tau) \\ + (\alpha \cos \tau + 2 \alpha^2 \cos^2 \tau + \alpha^2 + \alpha^3 \cos \tau + \alpha^3 \cos^3 \tau) = 0. \end{aligned} \quad (21)$$

When $\lambda = 0$, Equation (21) gives conditions necessary for a saddle-node bifurcation. The resulting equation may be factored into three conditions:

$$\alpha = 0, \quad (22)$$

$$\alpha = \frac{-\cos \tau}{1 + \cos^2 \tau}, \quad (23)$$

$$\alpha = \frac{-1}{\cos \tau}. \quad (24)$$

We can similarly set $\lambda = i\omega$ to obtain conditions necessary for a Hopf bifurcation. Omitting extraneous roots, we obtain:

$$\alpha = -\frac{1}{3 \cos \tau}, \quad \cos^2 \tau < \frac{1}{2}. \quad (25)$$

Simulation reveals that the limit cycle created in the Hopf bifurcation (25) is unstable. Equations (22–25) represent stability boundaries for the in-phase mode $x_1 \equiv x_2$ in the $\cos \tau - \alpha$ (or equivalently, the $\tau - \alpha$) parameter plane (Figure 1).

In order to check the stability results in Figure 1 and to confirm the validity of our approximations (both from averaging and from Taylor expanding the time delay terms), we numerically simulated Equations (1–2). The delay terms in Equations (1–2) require that initial conditions be given for the time interval between $-\tau$ and 0. We handled this by allowing the two oscillators to run uncoupled from $t = -\tau$ to $t = 0$. This was accomplished by specifying $x(-\tau)$ and $\dot{x}(-\tau)$ and thus allowed us to obtain an interval of initial conditions $\mathbf{x}(t) = \boldsymbol{\phi}(t)$, $-\tau \leq t \leq 0$. Then at time $t = 0$, we started numerically integrating the coupled delay equations, which require that we take into account what happened τ time units ago. Here we use a fourth order Runge–Kutta scheme with fixed step size, appropriately modified to account for delay [13]. In order to avoid unnecessarily long runs, we began close to the equilibrium point whose stability we were investigating. For example, in the case of the in-phase mode, we took $x_1 \approx x_2$, $\dot{x}_1 \approx \dot{x}_2$. A point in $\tau - \alpha$ parameter space is said to be stable if the trajectory

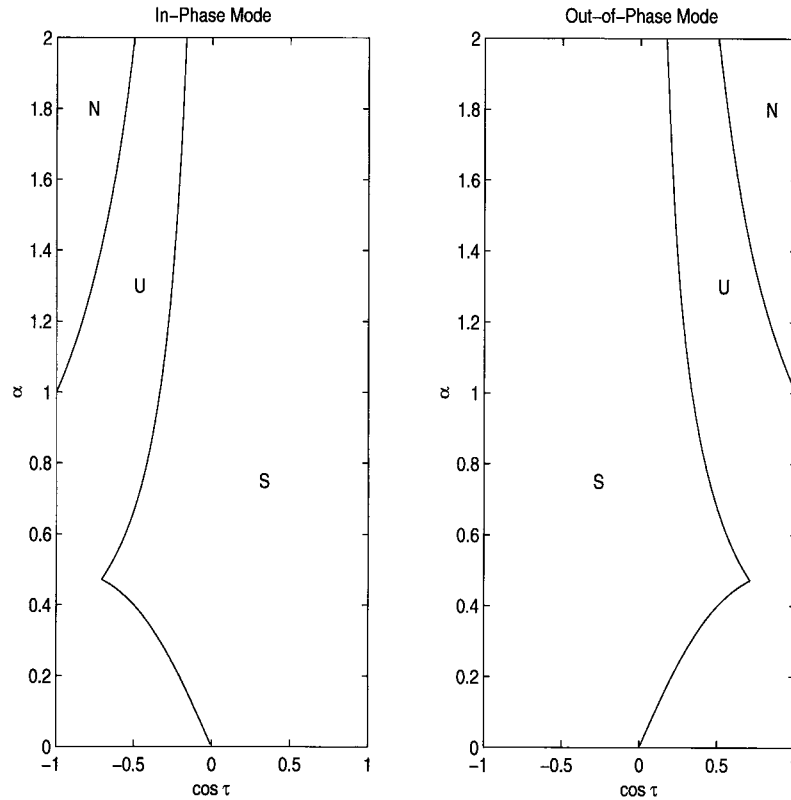


Figure 1. Stability of the in-phase and out-of phase modes: S = Stable, U = Unstable, N = does not exist.

in four-dimensional phase space continues to spiral into the in-phase mode. In this way we were able to confirm that the stability of the in-phase and out-of-phase modes agreed with the predictions of the analytical method shown in Figure 1.

Our treatment of Equations (1–2) involves three time scales: the period of the unforced, 2π ; the delay time, τ ; the slow time scale, $1/\varepsilon$. Our approximations should really be valid only when $\varepsilon \ll 1$ and where $\tau = O(1)$, that is, we have assumed $\varepsilon\tau \ll 1$. For larger values of ε , for example $\varepsilon = 0.5$, the analytical stability curves of the slow-flow equations do not give nearly as good agreement as when $\varepsilon = 0.1$. The larger the value of ε , the worse the approximation becomes. This is reasonable because the method of averaging assumes that $\varepsilon \ll 1$ and the stability regions occur at τ values near 2 . Numerical agreement is best for small ε and when $\tau = O(1)$ (Figure 2). This agrees with the theoretical restriction that $\varepsilon\tau \ll 1$. The periodicity of the stability results in τ predicted by the analytical treatment of the slow-flow is also seen to be only approximate and will indeed break down for large enough values of τ .

4. Stability of the Out-of-Phase Mode

In addition to the in-phase mode, Equations (12–14) also possess an equilibrium which corresponds to the out-of-phase mode $x_1 \equiv -x_2$:

$$R_1 = R_2 = 2 \sqrt{1 - \alpha \cos \tau}, \phi = \pi, \quad 1 - \alpha \cos \tau > 0. \quad (26)$$

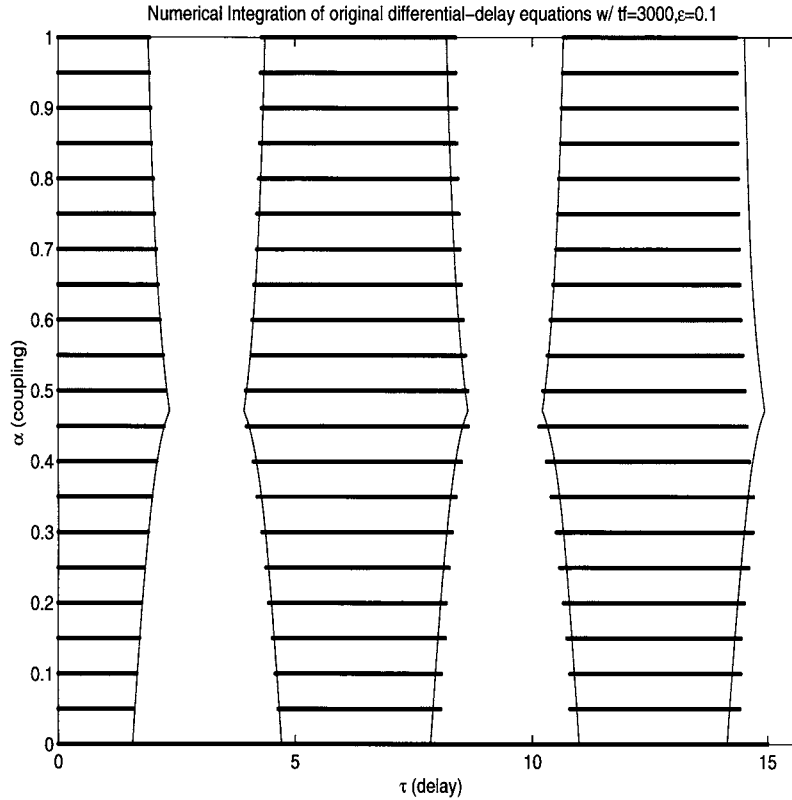


Figure 2. Stability of in-phase mode for $\varepsilon = 0.1$. Solid line is analytic prediction of stability given by (23) and (25); dots represent stability via numerical integration of (1–2).

In order to determine the stability of this mode we could proceed in an analogous fashion to that used for the in-phase mode. However, a more direct approach is available to us due to the symmetry discussed in Equations (16–18). The out-of-phase mode (26) maps to the in-phase mode (19) under the transformation (17), $\alpha \mapsto -\alpha$, $\tau \mapsto \tau + \pi$. But since the entire phase flow is invariant under this transformation, the stability of (26) is seen to be identical to that of (19) with the parameter change $\cos \tau \mapsto -\cos \tau$. That is, the out-of-phase mode has the same stability chart as the in-phase mode, reflected about the α -axis (Figure 1).

5. Unsymmetrical Modes

Having investigated the stability of the slow-flow equilibria corresponding to in-phase and out-of-phase modes, we now look for any other slow-flow equilibria, each of which corresponds to a periodic motion in the original equations (1–2). Our task is to solve the three Equations (12–14) for equilibrium values of R_1 , R_2 and ϕ . We solve (13) for R_1 , substitute the result into (14) and solve for R_2^2 . Call the result ‘equation A’. Then we solve (13) for R_1 and substitute the result into (12), giving a polynomial on R_2^2 . We substitute ‘equation A’ into this polynomial, giving an equation with no R_1 or R_2 in it. Algebraic and trigonometric simplification of the resulting equation gives:

$$\alpha^2 \sin^2 \tau \cos^4 \phi + (2\alpha^2 \sin^2 \tau - 1) \cos^2 \tau \cos^2 \phi + \cos^4 \tau (1 + \alpha^2 \sin^2 \tau) = 0. \quad (27)$$

Equation (27) is a quadratic on $\cos^2 \phi$. We may obtain up to four real values for $\cos \phi$, corresponding to eight values of ϕ . Of these eight, four must be rejected because they correspond to negative R_i values. The remaining four equilibria come in two pairs which map to each other under the transformation (15).

Bifurcations of these equilibria result from setting $\cos \phi = 1$ in Equation (27) since $\cos^2 \phi \leq 1$. This gives Equation (23) and its reflection in the symmetry (17). Bifurcations also occur in Equation (27) if the discriminant vanishes. This results in the condition

$$\alpha^2 = \frac{1}{8(1 - \cos^2 \tau)}, \quad \cos^2 \tau < \frac{1}{3}. \quad (28)$$

Equation (28) is displayed in Figure 3 along with the previously obtained bifurcation curves (23–25). Points P and Q in Figure 3 are defined as the points of intersection of curves (23) and (25), and of curves (23) and (28), respectively:

$$P: \cos \tau = -\frac{1}{\sqrt{2}}, \alpha = \frac{\sqrt{2}}{3}, \quad Q: \cos \tau = -\frac{1}{\sqrt{3}}, \alpha = \frac{\sqrt{3}}{4}. \quad (29)$$

The total number of slow-flow equilibria in Equations (12–14) depends on the parameters α and τ (Figure 3). The maximum number is six, consisting of the in-phase mode, the out-of-phase mode, and the four additional equilibria associated with Equation (27). Note that none of these additional equilibria can occur if the coupling α is sufficiently large.

We checked these results by numerically simulating Equations (12–14). In doing so we discovered that the equilibria discussed in this section undergo Hopf bifurcations in the regions marked ‘4’ and ‘6’ in Figure 3. In order to find the location of these Hopf bifurcations in the parameter plane of Figure 3, we linearized the slow-flow equations (12–14) about the equilibria given by Equation (27) and then set $\lambda = i\omega$ in the associated eigenequation. The resulting equations were too complicated algebraically to allow us to obtain closed form conditions for the Hopf bifurcations (even using computer algebra). Nevertheless we were able to treat the resulting equations numerically, revealing that the Hopf bifurcations occur along a curve which is displayed in Figure 4. This curve is approximately given by the empirical equation

$$\alpha = -0.045266 \cos^4 \tau + 0.286920 \cos^2 \tau + 0.3393455, \quad 0.238095 \leq \cos^2 \tau \leq 0.5. \quad (30)$$

As shown in Figure 4, the curve (30) reaches between point P and a point H on curve (28). The slow-flow limit cycles which are born in these Hopf bifurcations correspond to quasiperiodic motions in the original equations (1–2).

The unsymmetrical equilibria are born stable along PQ and lose their stability in a Hopf bifurcation (Figure 4). Thus they are only predicted to be stable in a very narrow region of parameter space. Given that averaging and Taylor expanding the time delay have made the analytical results only approximate, one might question the point of examining such regions of space. We thus chose $\tau = 2.26$ ($\cos \tau = -0.6359$), $\alpha = 0.45$, $\varepsilon = 0.01$, which is a point in parameter space in the middle of the region where the unsymmetrical equilibria are predicted to be stable, and numerically integrated the original differential-delay equations. Reassuringly, the unsymmetrical stable equilibria were found (Figure 5). This further validates the analytical treatment of our approximate system, Equations (12–14). We now proceed with finding the complete bifurcation set of the slow-flow equations (12–14).

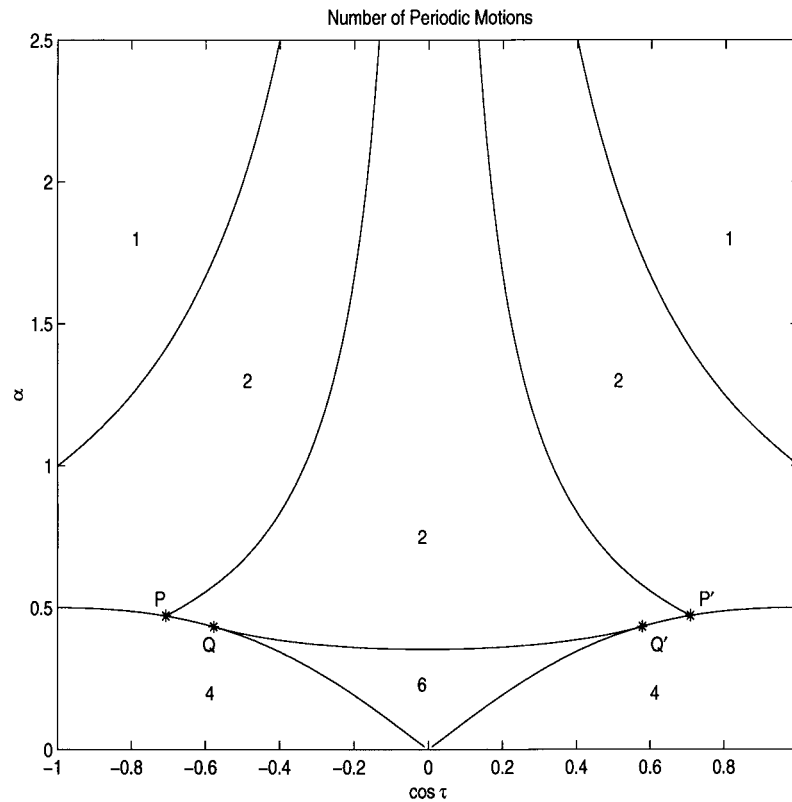


Figure 3. Number of periodic motions exhibited by the slow-flow (12–14). The displayed curves are the bifurcation equations (23), (24), (25), (27) as well as their reflections in the α -axis.

6. Unfolding Point P

In order to better understand the bifurcations which occur in the slow-flow equations (12–14), we magnify the region of parameter space around point P. This involves (i) expanding in power series the parameters α and τ about point P and the phase variables R_1 , R_2 and ϕ about the in-phase equilibrium point, then (ii) transforming the phase variables to local eigencoordinates (which involve a double zero eigenvalue at point P), then (iii) obtaining a power series approximation for the center manifold at P, and then (iv) transforming the resulting two-dimensional flow to normal form. This is a very complicated calculation which involved a lot of computer algebra. We give only the final form of the flow on the center manifold:

$$\begin{aligned} \dot{y} &= z, \\ \dot{z} &= y^3 \left(-\frac{1}{6} - \frac{175}{192} \sqrt{2} \mu - \frac{367}{288} \nu - \frac{1523}{256} \mu^2 + \frac{-317}{128} \nu^2 - \frac{1945}{384} \sqrt{2} \mu \nu \right) \\ &\quad + y^2 z \left(\frac{9}{2} + \frac{21}{4} \sqrt{2} \mu + \frac{19}{2} \nu - \frac{11763}{32} \mu^2 + \frac{729}{16} \nu^2 - \frac{1029}{16} \sqrt{2} \mu \nu \right) \\ &\quad + y \left(-\frac{1}{2} \sqrt{2} \mu + \frac{1}{9} \nu - \frac{3}{2} \mu^2 - \frac{1}{6} \nu^2 + \frac{-1}{6} \sqrt{2} \mu \nu \right) \end{aligned}$$

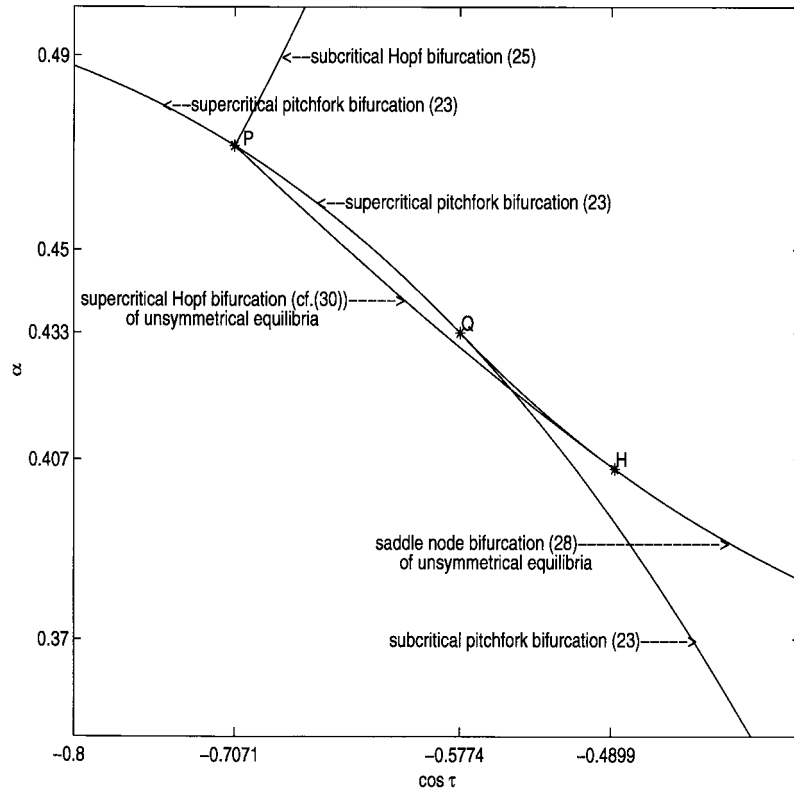


Figure 4. Enlargement of a region in Figure 3.

$$+ z \left(\frac{3}{2} \sqrt{2} \mu + v - \frac{1}{2} v^2 + \frac{3}{2} \sqrt{2} \mu v \right), \tag{31}$$

where μ and v are defined by the equations (cf. Equation (29))

$$\tau = \arccos \left(-\frac{1}{\sqrt{2}} \right) + v, \quad \alpha = \frac{\sqrt{2}}{3} + \mu. \tag{32}$$

Analysis of Equation (31) shows that there are six bifurcation curves which emanate from point P, a Takens–Bogdanov point [14]. See Figure 6 where these six curves are labeled A, B, C, D, E, F. Their description and approximate equations are found to be:

$$\text{A, C: pitchfork bifurcation, Equation (23): } \mu = \frac{\sqrt{2}}{9} v - \frac{13\sqrt{2}}{54} v^2, \tag{33}$$

$$\text{B: subcritical Hopf bifurcation, Equation (25): } \mu = -\frac{\sqrt{2}}{3} v + \frac{\sqrt{2}}{2} v^2, \tag{34}$$

$$\text{D: supercritical Hopf bifurcation, Equation (30): } \mu = \frac{\sqrt{2}}{6} v + \frac{47\sqrt{2}}{512} v^2, \tag{35}$$

$$\text{E: symmetry-breaking bifurcation: } \mu = \frac{17\sqrt{2}}{93} v + \frac{38173\sqrt{2}}{178746} v^2, \tag{36}$$

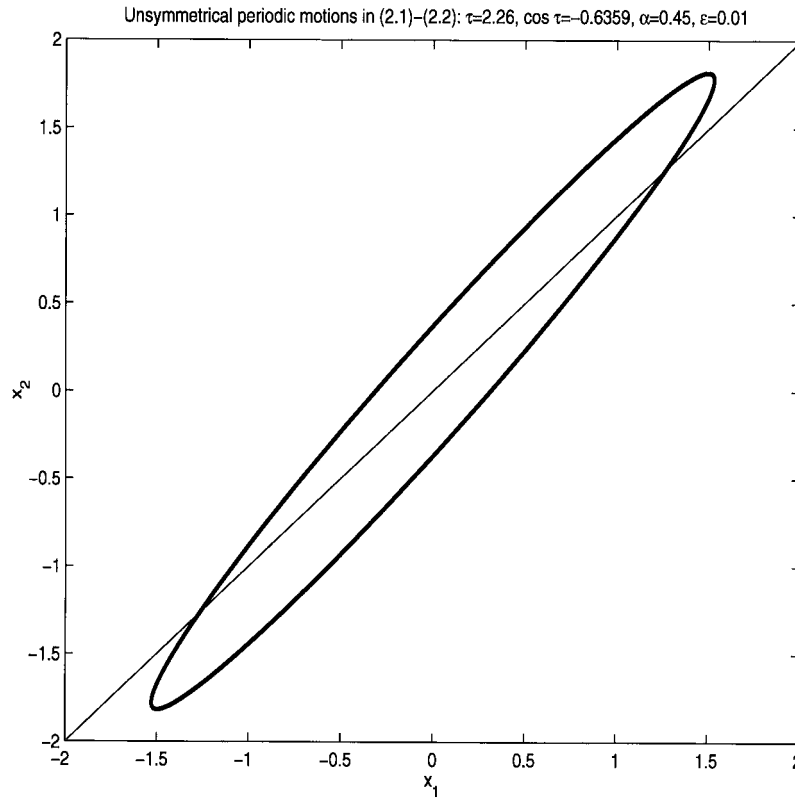


Figure 5. Unsymmetrical periodic motion in (1–2) which corresponds to an unsymmetrical equilibrium in (12–14). The initial condition used to generate the interval of delay values is $R_1 = 1.5253234$, $R_2 = 1.8161932$, $\phi = 0.20669649$. Equations (3) are also plotted. The other unsymmetrical equilibrium exists under $(x_1, x_2) \mapsto (x_2, x_1)$.

F: limit cycle fold: $\mu = 0.26606\nu$. (37)

In curve E, the symmetry-breaking bifurcation, a pair of stable limit cycles is replaced by a single larger stable limit cycle. In curve F, the limit cycle fold, a pair of limit cycles, one stable and one unstable, coalesce. It will be noted that the algebraic form of curve F involves an approximate decimal, in contrast to the expressions for the other bifurcation curves. In fact a closed form expression for this constant is known in terms of elliptic integrals, but is omitted here for brevity. The details by which Equations (33–37) are obtained, which involve Melnikov and elliptic integrals, are omitted here, but are included in the doctoral thesis of the first author [15]. Figure 7 shows a schematic of the bifurcation sequence obtained by moving through the parameter space near point P.

7. Unfolding Point Q

Recall that point Q is defined as the point where the double saddle-node bifurcation curve (28) joins with the in-phase mode pitchfork bifurcation curve (23), which occurs at

$$\cos \tau = \frac{-1}{\sqrt{3}}, \quad \alpha = \frac{\sqrt{3}}{4}. \tag{38}$$

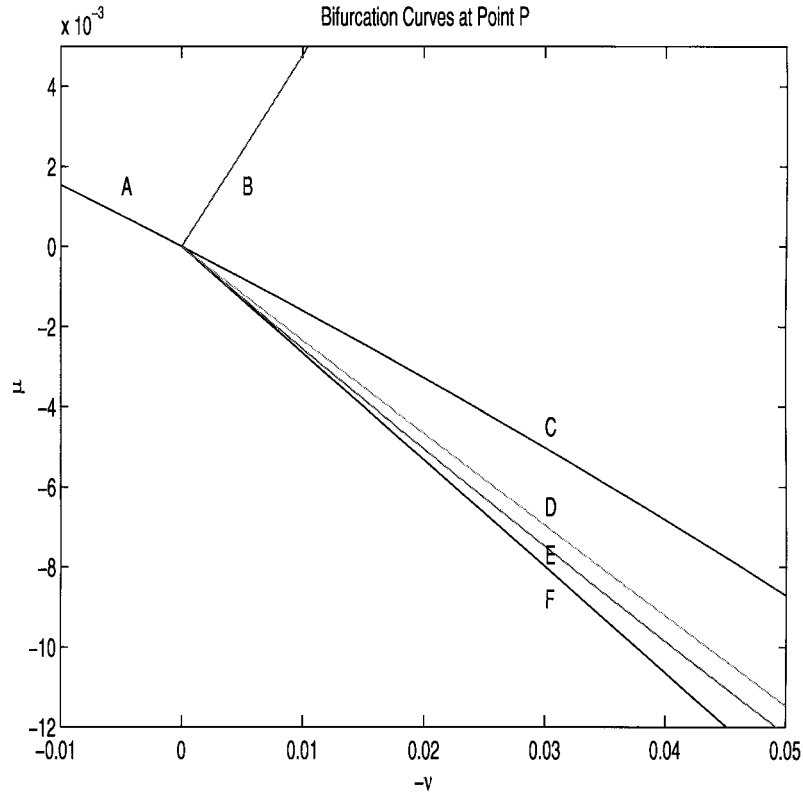


Figure 6. Bifurcation curves at point P obtained via center manifold analysis and normal forms. The equations for curves A, B, C, D, E, F are given in (33–37). Each of these curves separates regions of parameter space containing qualitatively distinct phase portraits, see Figure 7.

As with point P, we can similarly find the analytical stability curves coming in and out of point Q. The resulting equation describes the flow on the center manifold. We obtain the following expression:

$$\begin{aligned} \dot{z}_1 = & -2z_1^5 \\ & + \left(\frac{2788123\sqrt{3}}{19440}\mu - \frac{94267\sqrt{2}}{5184}v - \frac{35604121\sqrt{6}}{38880}\mu v + \frac{360207083}{19440}\mu^2 - \frac{47251}{1080}v^2 \right) z_1^5 \\ & + \left(\frac{-400\sqrt{3}}{27}\mu + \frac{23\sqrt{2}}{9}v + \frac{1154\sqrt{6}}{9}\mu v - \frac{45520}{27}\mu^2 - \frac{15}{2}v^2 \right) z_1^3 \\ & + \left(\frac{-4\sqrt{3}}{3}\mu + \frac{\sqrt{2}}{2}v + \frac{10\sqrt{6}}{3}\mu v - \frac{128}{3}\mu^2 + \frac{1}{4}v^2 \right) z_1, \end{aligned} \tag{39}$$

where (cf. Equation (29))

$$\tau = \cos^{-1} \left(\frac{-1}{\sqrt{3}} \right) + v,$$

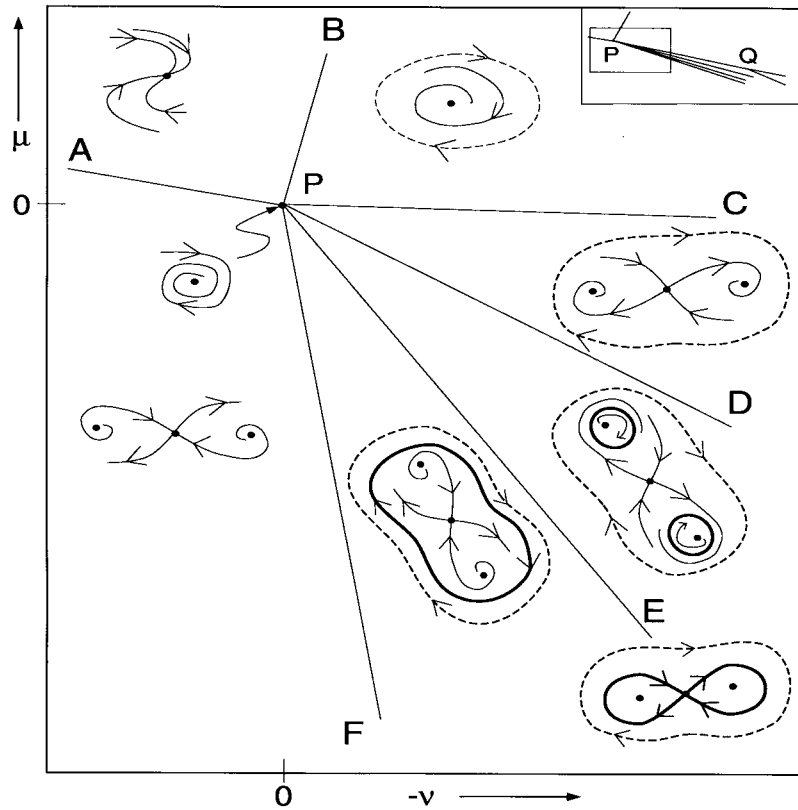


Figure 7. Schematic diagram showing the qualitatively distinct center manifold phase portraits found in the parameter space near point P. Note that in addition to all these steady states, the phase space also contains a stable equilibrium corresponding to the out-of-phase mode. Note that the curves are drawn distorted for better viewing, cf. Figure 6 and Equations (33–37).

$$\alpha = \frac{\sqrt{3}}{4} + \mu. \tag{40}$$

We expect very degenerate behavior at this point since the cubic term in the normal form switches from negative to positive as the bifurcation switches from supercritical to subcritical and this is indeed what the normal form shows. The bifurcation curves are found to be

$$\mu = \frac{\sqrt{6}}{8}v - \frac{5\sqrt{3}}{16}v^2 + O(v^3), \tag{41}$$

$$\mu = \frac{\sqrt{6}}{8}v + \frac{\sqrt{3}}{4}v^2 + O(v^3), \quad v < 0 \tag{42}$$

for the in-phase and double saddle-node local bifurcation curves, respectively.

8. The Completed Bifurcation Set

Having unfolded points P and Q, we now turn toward piecing together the entire bifurcation set of Equations (12–14). Although we have an implicit representation for point H, we were

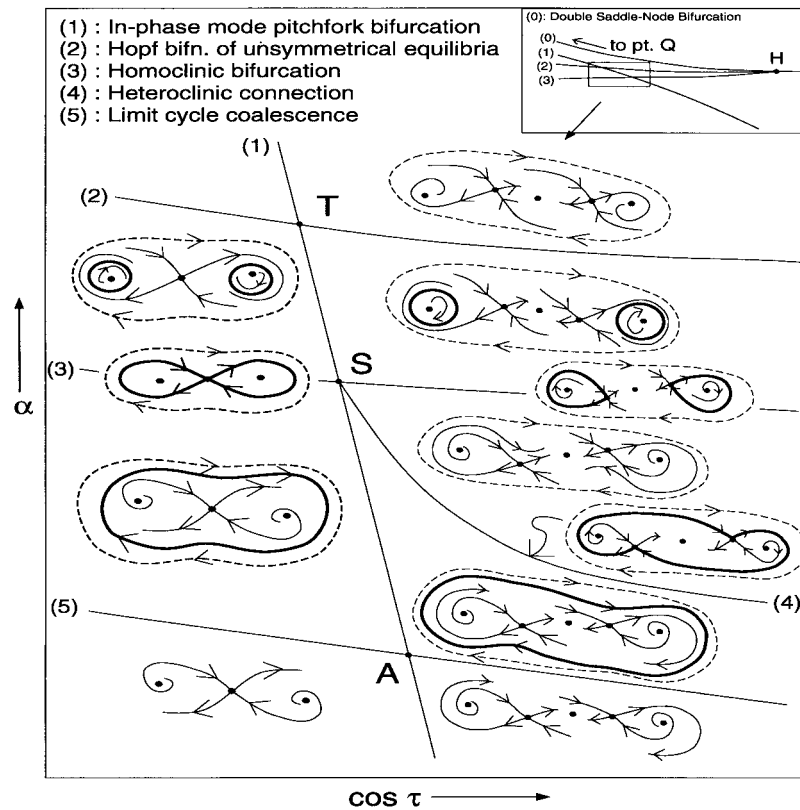


Figure 8. Bifurcation set (numerical) near points T, S, A. The out-of-phase mode exists (and is stable) throughout. The third eigendirection is (nearly) normal to the page and has negative eigenvalue. Note that curve (1) is drawn distorted for better viewing.

not able to write it in normal form using unfolding parameters (as we did with points P and Q); however, numerically simulating the flow on the center manifold at point H and the slow-flow equations near point H allowed us to conclude that point H is a Takens–Bogdanov point but of a different kind than point P [14]. Thus the Hopf bifurcation and the homoclinic bifurcation curves which emanate from point P (Figures 6 and 7) terminate at point H.

Numerical simulation and consistency arguments lead us to conjecture that at the point where the homoclinic bifurcation curve emanating from point P crosses the in-phase subcritical pitchfork bifurcation curve, we have the beginning of a curve of heteroclinic connections involving the two unsymmetrical equilibria (Figure 8), which gives rise to a large stable limit cycle. Consistency arguments and numerical simulation again allow us to conclude that this bifurcation curve of heteroclinic connections and the bifurcation curve along which the limit cycles coalesce cannot terminate at point H.

We note that due to the type of Takens–Bogdanov bifurcation that occurred at point H, there exists a curve extending to the right of point H satisfying $\Sigma \lambda_i = 0$ where λ_i are the two principal eigenvalues. Since this is just the trace of the matrix corresponding to these eigenvalues, we will refer to the curve as the $\mathbf{tr} = 0$ curve. This curve may be thought of as an extension of the unsymmetrical Hopf bifurcation curve and indeed, we used this extension to calculate the empirical equation for the Hopf bifurcation, given by Equation (30).

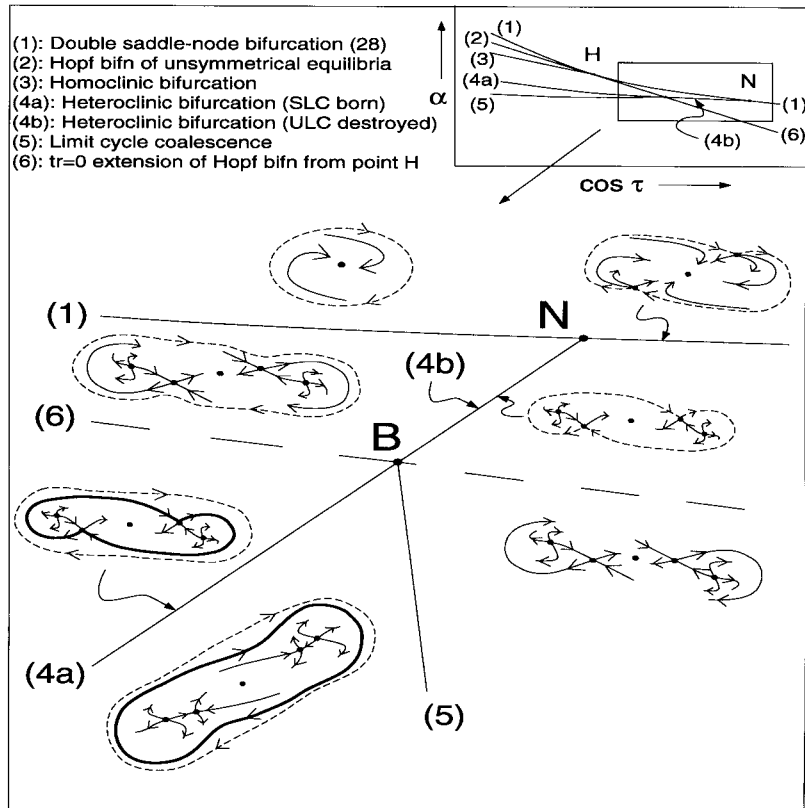


Figure 9. Bifurcation set and phase portraits near points N with curves drawn distorted for better viewing. Note that the phase portraits above and below curve (6) are identical and are thus only drawn once. Also, the third eigendirection is contracting and in a direction (nearly) normal to the page.

This extension goes from H to H' and enters tangent to (28) at the respective points. The significance of this curve is that the heteroclinic and limit cycle fold curves must intersect it. For values of α below the $\text{tr} = 0$ extension, the limit cycle born in the heteroclinic bifurcation must be stable; however, for values of α above the $\text{tr} = 0$ extension, the limit cycle born in the heteroclinic bifurcation must be *unstable*. Thus the limit cycle fold curve and the heteroclinic bifurcation curves must join together at the $\text{tr} = 0$ extension curve with only the heteroclinic bifurcation curve continuing on the other side (Figure 9).

To determine the fate of the heteroclinic and limit cycle fold curves, we examine the special case when $\tau = \pi/2$. The planes $\phi = \pm\pi/2$ are invariant planes and due to the nature of heteroclinic orbit (Figure 10), a consistency argument leads us to conjecture that the heteroclinic bifurcation curve could not possibly exist at a value of $\tau = \pi/2$. Thus we conjecture that there exists a point N on the double saddle-node bifurcation curve, H-H', lying neither close to H nor to $\tau = \pi/2$ at which point the heteroclinic bifurcation curve terminates. Although this occurrence may seem highly unusual, it has been observed in similar systems [14, 16]. A similar argument holds when $\tau = 3\pi/2$. The completed bifurcation set is given in Figure 11.

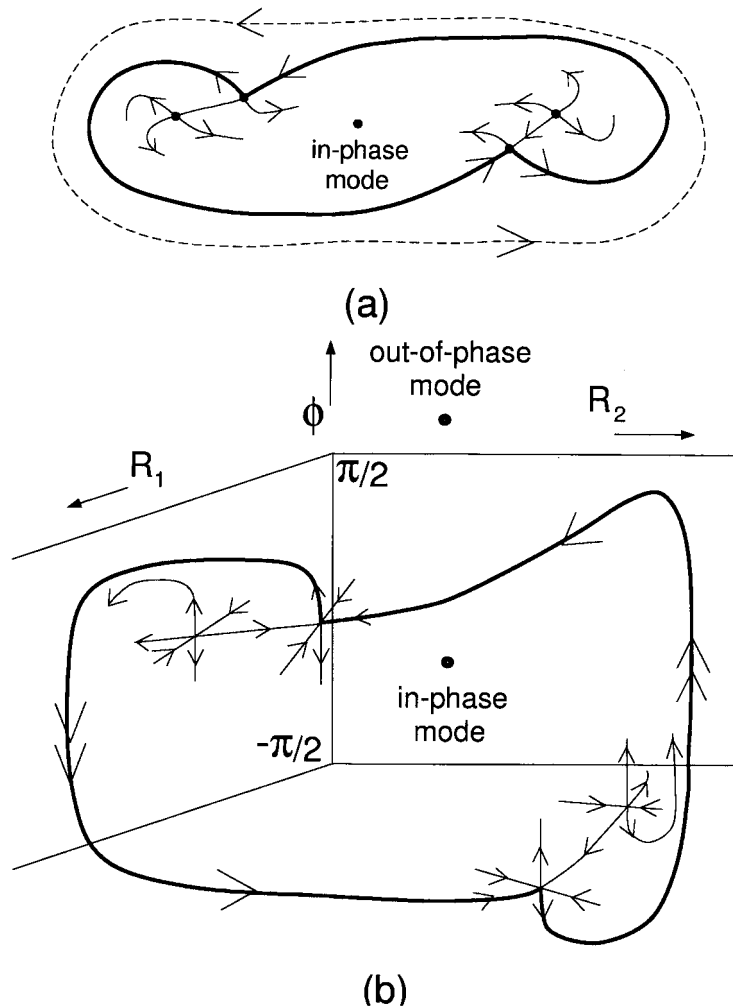


Figure 10. Heteroclinic connection close to H-H'. (a) shows the two-dimensional projection of this connection observed in Figure 8 while (b) shows the full three-dimensional connection.

9. Discussion

Perhaps the most significant result of this work is the conclusion that both the in-phase and out-of-phase modes are stable for values of $\cos \tau$ close to zero, i.e., for delays of about 1/4 of the uncoupled period of the oscillators, see Figure 1. We have seen good agreement between numerical integration results and the analytical results for small values of $\varepsilon \tau$ and this agreement deteriorates as ε increases. Also, the parameter τ always appears in the form $\cos \tau$ in the slow-flow (12–14), leading to the prediction that the dynamical behavior exhibits a periodic dependence on τ . Recent research work which does not assume that $\varepsilon \tau$ is small has shown that this prediction is only approximately true [17, 18].

The elaborate bifurcation sequences which were found to be present in this system occur over a very small region of parameter space, and hence may be difficult to observe in an associated physical system. Nevertheless these bifurcations are important because they explain how dynamical transitions occur between the larger regions of parameter space.

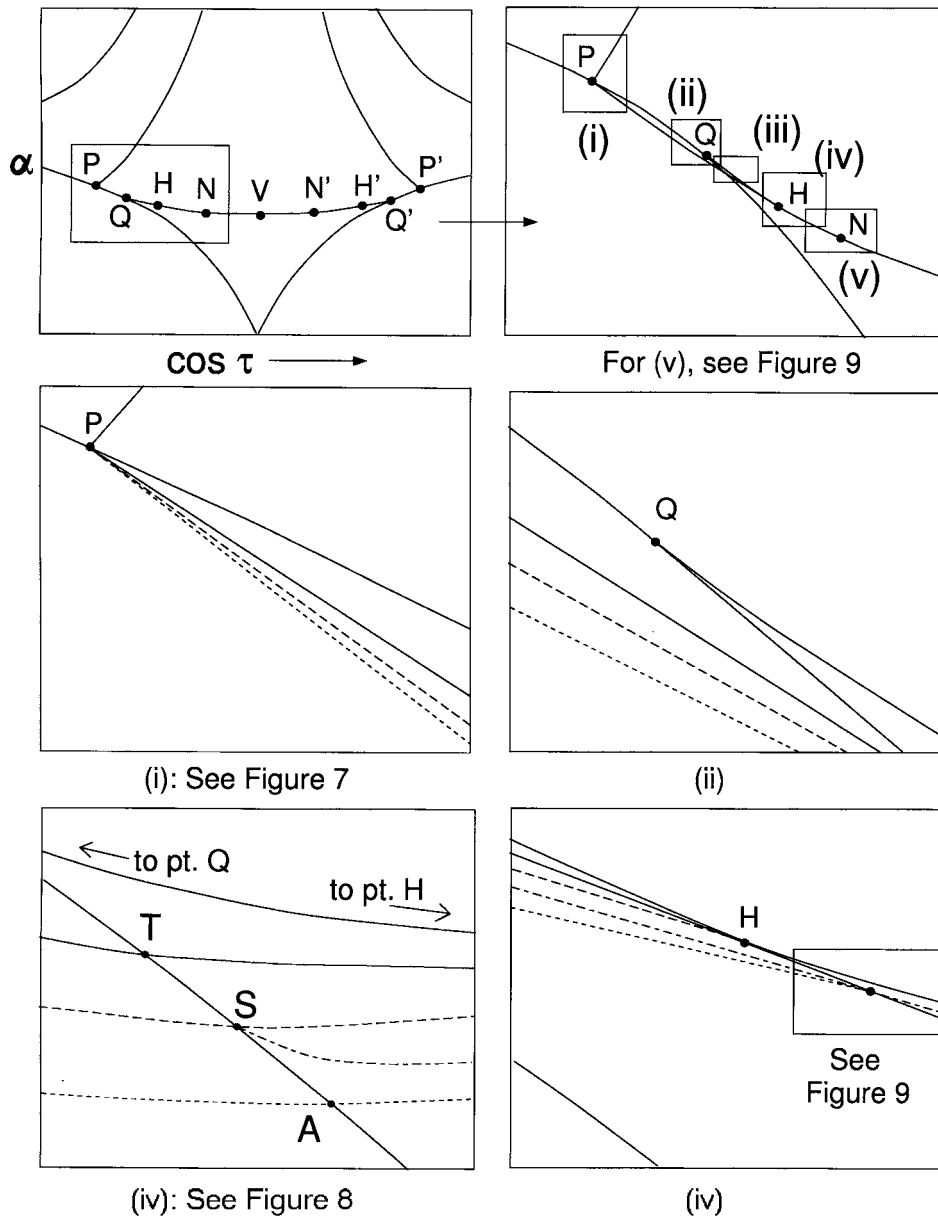


Figure 11. Complete bifurcation set of Equations (12–14). For the top left frame, cf. Figure 3 and for the top right frame, cf. Figure 4. Note also that the same bifurcation curves exist under $\cos \tau \mapsto -\cos \tau$.

Acknowledgments

The authors wish to thank Professor Rick Compton for proposing this problem, and Professors Steven Strogatz and John Guckenheimer for helpful suggestions.

References

1. Lynch, J. J. and York, R. A., 'Stability of mode locked states of coupled oscillator arrays', *IEEE Transactions on Circuits and Systems* **42**, 1995, 413–417.
2. Lynch, J. J., 'Analysis and design of systems of coupled microwave oscillators', Ph.D. Thesis, Department of Electrical and Computer Engineering, University of California at Santa Barbara, 1995.
3. York, R. A. and Compton, R. C., 'Experimental observation and simulation of mode-locking phenomena in coupled-oscillator arrays', *Journal of Applied Physics* **71**, 1992, 2959–2965.
4. York, R. A., 'Nonlinear analysis of phase relationships in quasi-optical oscillator arrays', *IEEE Transactions on Microwave Theory and Techniques* **41**, 1993, 1799–1809.
5. Wirkus, S. and Rand, R., 'Dynamics of two coupled van der Pol oscillators with delay coupling', in *Proceedings of DETC'97, 1997 ASME Design Engineering Technical Conferences*, Sacramento, CA, September 14–17, ASME, New York, 1997, Paper No. DETC97/VIB-4019.
6. Wirkus, S. and Rand, R., 'Bifurcations in the dynamics of two coupled van der Pol oscillators with delay coupling', in *Proceedings of DETC'99, 1999 ASME Design Engineering Technical Conferences*, Las Vegas, NV, September 12–15, ASME, New York, 1999, Paper No. DETC99/VIB-8318.
7. Rand, R. H. and Holmes, P. J., 'Bifurcation of periodic motions in two weakly coupled van der Pol oscillators', *International Journal of Non-Linear Mechanics* **15**, 1980, 387–399.
8. Storti, D. W. and Rand, R. H., 'Dynamics of two strongly coupled van der Pol oscillators', *International Journal of Non-Linear Mechanics* **17**, 1982, 143–152.
9. Storti, D. W. and Rand, R. H., 'Dynamics of two strongly coupled relaxation oscillators', *SIAM Journal on Applied Mathematics* **46**, 1986, 56–67.
10. Chakraborty, T. and Rand, R. H., 'The transition from phase locking to drift in a system of two weakly coupled van der Pol oscillators', *International Journal of Non-Linear Mechanics* **23**, 1988, 369–376.
11. Reddy, D. V. R., Sen, A., and Johnston, G. L., 'Time delay induced death in coupled limit cycle oscillators', *Physical Review Letters* **80**, 1998, 5109–5112.
12. Strogatz, S. H., 'Death by delay', *Nature* **394**, 1998, 317–318.
13. Hairer, E., Nørsett, S. P., and Wanner, G., *Solving Ordinary Differential Equations I: Nonstiff Problems*, Springer-Verlag, Berlin, 1987.
14. Guckenheimer, J. and Holmes, P., *Nonlinear Oscillations, Dynamical Systems, and Bifurcations of Vector Fields*, Springer-Verlag, New York, 1983.
15. Wirkus, S., 'The dynamics of two coupled van der Pol oscillators with delay coupling', Ph.D. Thesis, Center for Applied Mathematics, Cornell University, 1999.
16. Holmes, P. and Rand, D., 'Bifurcations of the forced van der Pol oscillator', *Quarterly of Applied Mathematics* **35**, 1978, 495–509.
17. Moon, F. C. and Johnson, M. A., 'Nonlinear dynamics and chaos in manufacturing processes', in *Dynamics and Chaos in Manufacturing Processes*, F. C. Moon (ed.), Wiley, New York, 1998, pp. 3–32.
18. Yeung, M. K. S. and Strogatz, S., 'Time delay in the Kuramoto model of coupled oscillators', *Physical Review Letters* **82**, 1999, 648–651.